Molecular-dynamics simulation of the trivalent europium ion doped in sodium disilicate glass: Electronic absorption and emission spectra

G. Cormier and J. A. Capobianco*
Department of Chemistry and Biochemistry, Concordia University, 1455 de Maisonneuve Boulevard West, Montréal, Canada H3G 1M8

C. A. Morrison
U.S. Army Research Laboratory, Adelphi, Maryland 20783

A. Monteil
Université de Lyon I, 69622 Villeurbanne, France

(Received 5 April 1993; revised manuscript received 26 August 1993)

We report the simulation of the optical absorption and emission spectra of the Eu^{3+} ion doped in a sodium disilicate glass. A model of this glass was previously simulated by the molecular-dynamics technique. We employ a full treatment, including J mixing, of the point-charge crystal-field method developed for doped crystalline materials in order to simulate (1) the $^5L_6$,$^5D_{3,2,1,0} \leftarrow {}^7F_{0,1}$ absorption spectrum and (2) the $^5D_0 \rightarrow {}^7F_{0-6}$ emission spectrum of the Eu^{3+} ion. This produces simulated spectra with correct energies and relative intensities. A comparsion to experimental room-temperature absorption and fluorescence spectra of the corresponding laboratory glass is presented. By combining the simulated structural model with the calculated optical spectra, we are able to investigate spectra-structure correlations of doped inorganic glasses.

I. INTRODUCTION

It is well known that optical spectra of rare-earth ions doped in glasses consist of a superposition of contributions from individual ions distributed amongst the entire ensemble of local environments. As such, the spectra exhibit inhomogeneous broadening and information about the local environment of the rare-earth ions is exceedingly difficult to obtain. Energy-selective spectroscopic techniques, such as laser-induced fluorescence line narrowing (FLN),[1-4] have been used to overcome the difficulty presented by the inhomogeneous broadening of the fluorescence peaks. In this technique, energy subsets of the whole ensemble of doped ions are resonantly excited by a narrow band source, such as a tunable dye laser. Thus, fluorescence observed from the sample originates from this subset. Two different approaches have been taken to extract structural information from FLN spectra: (1) Brecher and Riseberg[1,5] have compared FLN spectra of Eu^{3+} in silicate and fluoroberyllate glasses with energy levels derived from a simple point-charge model of ligands surrounding a Eu^{3+} ion in a distorted polyhedra, (2) Brawer and Weber[6-10] simulated Eu^{3+}-doped fluoroberyllate glasses using Monte Carlo and molecular-dynamics (MD) techniques. Under a point-charge model, Brawer and Weber examined the range and distribution of energy-level splittings of the ground-state manifold of the Eu^{3+} ion. Certain simplifications were introduced in their calculations: (1) only the $^7F_0$ and $^7F_1$ manifolds were treated, (2) no J mixing was assumed, (3) only ligands within 2.75 Å were considered in the point-charge calculation, (4) only the second-order crystal-field parameters were included in the calculation, and (5) only relative energy-level splittings of the electronic manifolds were inferred. Qualitative observations were made which agreed with the results of the experiment. Firstly, the range and distribution of crystal-field energy levels agreed with observations of both broadband and FLN spectra. Secondly, the high-energy asymmetry of the $^5D_0 \rightarrow {}^7F_0$ emission profile together with the magnitude of the inhomogeneous broadening of the $^5D_0 \rightarrow {}^7F_1$ band were both successfully predicted. Finally, the overall linewidths and average energy-level splittings were predicted to be smaller in the modified glasses than in the BeF_2 glass.

In retrospect, Weber[11] felt that although a qualitative agreement was obtained by the simple electrostatic model, accurate calculations, and simulations of both the local structure and electronic energy levels would be required to quantitatively predict and interpret optical spectra of glasses.

In a previous article,[12] we analyzed the local structure of Eu^{3+} ions doped in simulated amorphous silica (SiO_2:Eu^{3+}) and sodium disilicate glass ($Na_2O \cdot 2SiO_2$:Eu^{3+}). These glasses were simulated by the MD technique.[13] We showed that the Eu^{3+} ions are found as quasimolecular complexes[14] and have average coordination numbers of 4 and 6 in SiO_2 and $Na_2O \cdot 2SiO_2$ glasses, respectively. We also showed that the local structure of the europium ions is influenced to a greater degree by bonding and energetic requirements than by the topology of the silicate framework.

In this paper, we examine the relevancy of making correlations between the local environment and the calculated spectral features of the Eu^{3+} ions doped in simulated $Na_2O \cdot 2SiO_2$ glass. We shall employ a full treatment, including J mixing, of the point-charge crystal-field method developed for doped crystalline materials[15-18] in

order to simulate (1) the $^5L_6, ^5D_{3,2,1,0} \leftarrow ^7F_{0,1}$ absorption spectrum and (2) the $^5D_0 \rightarrow ^7F_J$ ($J=0-6$) emission spectrum of the Eu^{3+} ion. The method employed is related to the "lattice-summation" technique,[19,20] where crystal-field parameters are derived from the interaction between the impurity ion and the electrostatic potential of the surrounding lattice. Knowing the position and charge of each atom, we can calculate the electrostatic potential at the rare-earth site by summing each individual atomic contribution. The calculated crystal-field parameters are used (1) in the calculation of the splitting of each J manifold and (2) in the calculation of the transition probabilities between all individual components of each J manifold. In effect, this gives us a simulated emission or absorption spectrum with correct energies and relative intensities. Experimental data obtained from absorption and fluorescence spectroscopy of the corresponding laboratory glass are presented.

II. THE SIMULATED GLASS

The molecular-dynamics (MD) method used to perform the simulation of the atomic structure of the doped glass is based on the numerical integration of the classical Newtonian equations of motion. The force law used in the calculation is derived from a pairwise (two-body) ionic potential which includes a Pauling repulsive term. It is of the same form as that described by Mitra and Hockney[21,22] and is found to be

$$F(r_{ij}) = \frac{q_i q_j}{r_{ij}^2}\left[1+\text{sign}(q_i q_j)\left[\frac{\sigma_i+\sigma_j}{r_{ij}}\right]^n\right], \quad (1)$$

where q_i and q_j are the ionic charges, σ_i and σ_j are the ionic radii of the atoms i and j, n is a measure of the hardness of the repulsion, and r_{ij} is the distance between atoms i and j. Charges, radii, and n were determined empirically such that they reproduce the observed short-range structure of the corresponding laboratory glass.[23,24] The composition of the simulated glass is given in Table I, with other relevant parameters. A cubic cell was used in these calculations with periodic boundary conditions to eliminate the possibility of surface effects. The simulation was performed on an IRIS 4D/25G workstation from Silicon Graphics. To insure a statistical distribution of Eu^{3+} environments, we have simulated a total of 75 glass configurations, each containing two Eu^{3+} ions.

Details concerning the simulation procedure and the potential parameters are found in a previous paper.[12]

TABLE I. Simulation parameters for the $Na_2O \cdot 2SiO_2:Eu^{3+}$ glass.

	$Na_2O \cdot 2SiO_2:Eu^{3+}$
Molar fract. of Na_2O (x)	0.33
Number of O ions	337
Number of Si ions	134
Number of Na ions	132
Number of Eu ions	2
Simulated density (g/cm^3)	2.507
Oxygen molar volume ($cm^3/mol\ O^{2-}$)	14.499
Length of box side (Å)	20.085

III. THE LABORATORY GLASS

Two samples of Eu^{3+}-doped sodium disilicate glasses were prepared. Sample "A" has a Eu^{3+} concentration of 0.94 wt. % (8.79×10^{19} ions/cm^3), and sample "B" has a Eu^{3+} concentration of 5.0 wt. % (4.52×10^{20} ions/cm^3). The preparation procedure was the following: (1) grounding appropriate quantities (see Table II) of analytical reagent grade oxides and carbonate (SiO_2, Na_2CO_3, Eu_2O_3), (2) melting the powders at 1200 °C for 1 h in a platinum-rhodium crucible in an electrically heated furnace, (3) fritting in deionized water then drying, crushing, and remelting at 1200 °C for 1 h, and (4) annealing for a period of 1 h at 500 °C and then slowly air cooling.

Practical considerations dictated the use of two different samples. The 5% sample was studied in absorption in order to obtain a better signal-to-noise ratio, whereas the 1% sample was studied in emission in order to minimize possible energy transfer between the Eu^{3+} ions.

IV. SPECTROSCOPY OF THE LABORATORY GLASS

A room-temperature absorption spectrum of sample B was recorded between 350 and 600 nm using a Perkin-Elmer Lambda 5 spectrophotometer (resolution, 1 nm).

Room- and nitrogen-temperature broadband emission spectra were taken by exciting sample A with the 514.5-nm line of a Coherent CR-18 argon-ion laser. The fluorescence line narrowed (FLN) spectra were excited using a Spectra Physics 375 dye laser operating with rhodamine 6G (Exciton) pumped by the 514.5-nm line of the argon-ion laser. The concentration of the dye was 10^{-3} mol/dm^3 in ethylene glycol (Aldrich, spectrophotometric, 99+%). The dye laser has a typical linewidth of 2 cm^{-1} full width at half maximum (FWHM) over the tuning range of 573–581 nm used in this study. The emission spectra were recorded by using a Jarrell-Ash 1-m Czerny-Turner double monochromator. The emission signal was monitored by an RCA-C31034-02 photomultiplier. The photomultiplier was thermoelectrically cooled so that its background dark rate was below 2 counts/s. The photomultiplier signal was processed by a preamplifier, model SR-440 (Stanford Research Systems).

TABLE II. Composition of the experimental $Na_2O \cdot 2SiO_2:Eu^{3+}$ glasses.

	Sample "A"		Sample "B"	
	Mass (g)	% molar	Mass (g)	% molar
SiO_2	5.250 93	65.99	5.000 0	66.05
Na_2CO_3	4.750 84	33.85[a]	4.410 0	33.02[a]
Eu_2O_3	0.077 6	0.17	0.398 9	0.93

[a]The molar percentage reported is for the oxide Na_2O, which results from the high-temperature decomposition of the carbonate Na_2CO_3.

A two-channel gated photon counter, Model SR-400 (Stanford Research Systems) was used as the data acquisition system. The signal was recorded under computer control using the Stanford Research Systems' SR-465 software data acquisition/analysis system. The low-temperature spectra were acquired at 77 K using a Janis Research ST-VP-4 continuous flow cryostat.

V. CRYSTAL-FIELD ANALYSIS

The crystal-field Hamiltonian that describes the interaction of the Eu^{3+} ion with the host lattice can be written as

$$\mathcal{H}_{CEF}=\sum_{nm} A^{*}_{nm} \sum_{i} r_i^n C_{nm}(\hat{r}_i) , \tag{2}$$

where the first sum covers those values of n and m allowed by the symmetry of the site of the rare earth. With n even, Eq. (2) is used to calculate the crystal-field splittings; for n odd, it is used to calculate transition probabilities. The second sum is over $i=6$ electrons of the $4f^6$ configuration of the Eu^{3+} ion. The simplest description of the crystal field uses the point-charge model, in which the atoms of the lattice surrounding the rare-earth ion are described by point charges. This model neglects both the finite spatial extent of the ligand charge density and the wave function overlap of the optically active $4f$ electrons with the ligands.[25] For point charges, eq_j located at $\mathbf{R}_j$, the crystal-field components, A_{nm} of Eq. (2) are given by

$$A_{nm}=-\frac{e^2}{4\pi\varepsilon_0}\sum_j q_j \frac{C_{nm}(\hat{R}_j)}{R_j^{n+1}} . \tag{3}$$

In Eqs. (2) and (3), the irreducible spherical tensors $C_{nm}(r)$ are related to the spherical harmonics $Y_{nm}(\theta,\phi)$.[26]

Using the atomic positions obtained from the molecular-dynamics simulation and by choosing appropriate ionic charges for each atom type, it is possible to calculate the crystal-field components, A_{nm}. Using the three-parameter theory of crystal fields proposed by Leavitt, Morrison, and Wortman,[15] the crystal-field parameters, B_{nm}, can be calculated.

The B_{nm} crystal-field parameters are directly related to the point symmetry of the local environment of the Eu^{3+} ion. For reasons which will be discussed in Sec. VIII, we have chosen to analyze the simulated structure using a C_2 point-group symmetry. From the crystal-field parameters B_{nm}, it is possible to calculate the crystal-field strength. A quantitative measure of the strength, S_{CF}, of the interaction between the rare-earth ion and the surrounding lattice can be obtained from the equation derived by Leavitt.[27]

The crystal-field strength is directly related to the splitting of the J manifolds due to the crystal field; in general, the larger the value of S_{CF}, the larger the splitting will be.

VI. INTENSITY CALCULATIONS AND BRANCHING RATIOS

Following Condon and Shortley,[28] the line strength S_{ab} of a radiative transition between individual components a and b, of J states A and B, is given by the square of the matrix element

$$S_{ab}=|\langle b|\mathbf{P}|a\rangle|^2 , \tag{4}$$

where $\mathbf{P}$ is the appropriate operator (electric or magnetic dipole).

Electric dipole intensity calculations were performed using the "full" Judd-Ofelt theory of induced electric dipole transitions.[29,30] This theory involves the calculation of the squared matrix elements of the electric dipole operator between crystal-field split eigenstates *including J* mixing. The effective electric dipole moment operator, used in the present calculations, is identical to Eq. (1) in Ref. 31. We can compute the necessary parameters found in this equation and subsequently calculate the line strength S_{ab}^{ED} using the methods proposed by Krupke[32] and by Morrison *et al.*[31] Within the electronic configuration $4f^n$, magnetic dipole transitions are parity allowed. Thus, the calculation of the line strength is more straightforward than for the electric dipole case. With the proper dipole moment operator, Eq. (4) can be directly used to give the magnetic dipole line strength S_{ab}^{MD}.[31] Finally, one must note that J mixing of eigenstates is included in the calculation of the magnetic dipole and electric dipole line strengths.

In order to calculate the intensity of line-to-line transitions in the simulated emission and absorption spectra, we will use (1) the oscillator strength between the individual components a and b, f_{ab}, for the absorption process:

$$f_{ab}=\frac{8\pi^2 mc\sigma_{ab}}{3h}\left[\left[\frac{(n^2+2)^2}{9n}\right]S_{ab}^{ED}+nS_{ab}^{MD}\right] \tag{5a}$$

and (2) the transition probability between the individual components a and b, A_{ab}^{ems}, for the emission process is given by

$$A_{ab}^{ems}=\frac{32\pi^3 e^2\sigma_{ab}^3}{3\hbar 4\pi\varepsilon_0}\left[\left[\frac{n(n^2+2)^2}{9}\right]S_{ab}^{ED}+n^3 S_{ab}^{MD}\right] . \tag{5b}$$

VII. SIMULATED SPECTRA

The following procedure was used to calculate electronic spectra of the Eu^{3+} ions doped in the simulated silicate glass. The bulk of the procedure is the same for the calculation of both emission and absorption spectra. Differences arise during discussions of line intensities.

A principal axis transformation of each of the 150 Eu^{3+} configurations[12] was performed to correlate the energy levels with the structure and charge distribution at each rare-earth site. Starting with a Eu^{3+} ion at the center of a Cartesian coordinate system representing the glass configuration, we can define the components of the

quadrupole moment tensor at the rare-earth site as a (3×3) matrix such that its quadratic form is

$$M_{ij}=\sum_{L}\left[\frac{q_L}{R_L^5}\cdot r_i r_j\right], \tag{6}$$

where a summation over the entire ensemble of L ligands is carried out. The parameters of the quadratic form are q_L, the electronic charge of ligand L, R_L, the distance separating ligand L from the Eu^{3+} ion, and $r_i r_j$, the x, y, or z components of the position of ligand L. This symmetric matrix M_{ij} is diagonalized and yields eigenvalues $\lambda_1,\lambda_2,\lambda_3$ and eigenvectors $\mathbf{A}_1$, $\mathbf{A}_2$, $\mathbf{A}_3$. The eigenvectors represent the principal axes of an ellipsoid. The magnitude of the major and minor axes are given by the eigenvalues. Sorting the eigenvalues such that $\lambda_1>\lambda_2>\lambda_3$ and rearranging the eigenvectors correspondingly permits us to carry out an alignment of each quadrupolar moment ellipsoid. By a similarity transformation,[33] we can apply the same rotation obtained through the alignment of the ellipsoids to each of the 150 glass configurations.

Once each of the glass configurations is aligned, we calculate the crystal-field parameters by a program which takes as input (1) the positions of all atoms with respect to the central Eu^{3+} ion and (2) the charges assigned to each atom type. It proceeds to determine the spherical tensors C_{nm} using a recursive method which calculates the associated Legendre polynomials. The C_{nm} parameters are used in the calculation of the crystal-field components A_{nm} using Eq. (3). The even-n A_{nm} are transformed into crystal-field parameters B_{nm} using the ρ_n parameters previously reported for Eu^{3+}.[15]

In order to generate a graphic representation of the simulated emission and absorption spectra, the calculated energies are collated and sorted. A Gaussian band shape is assigned to each of the energies. The spectral envelope, $\Xi(E)$, is given by

$$\Xi(E)=\frac{1}{\sqrt{2\pi}\cdot w\cdot N_0}\sum_{k=1}^{N_0}\sum_{a,b}I_{k,ab}^{\text{type}}\exp\left[-\frac{(E-E_{k,ab})^2}{2w^2}\right], \tag{7}$$

where the first sum is over the $N_0=150$ Eu^{3+} configurations and the second sum is over the 49 possible line-to-line $^5D_0\rightarrow{}^7F_J$ $(J=0-6)$ transitions for the emission spectrum or is over the (4×29) possible line-to-line $^5L_6$, $^5D_3$, $^5D_2$, $^5D_1$, $^5D_0\leftarrow{}^7F_{0,1}$ transitions for the absorption spectrum. The $E_{k,ab}$ are the line-to-line transition energies for each of the Eu^{3+} ions, such that $E_{k,ab}=|E_a-E_b|_k$. The width w of each individual Gaussian has been chosen to be ≈75 cm^{-1} for the emission spectrum and ≈100 cm^{-1} for the absorption spectrum. These widths were chosen such that the 150 Eu^{3+} ions of the simulated glass effectively represent the macroscopic ensemble of doped ions found in the experimental glass. The difference in these widths stems from the fact that two different types of experimental spectra (absorption and emission) were taken at different resolutions. The intensity parameters $I_{k,ab}^{\text{type}}$ are defined as the following:

$$I_{k,ab}^{\text{ems}}=F_{ab}^{\text{ems}}[(\beta_{k,ab})\cdot(A_{k,ab}^{\text{ems}})] \tag{8a}$$

with $A_{k,ab}^{\text{ems}}$ given in Eq. (5b), and

$$I_{k,ab}^{\text{abs}}=F_{ab}^{\text{abs}}\cdot f_{k,ab}\ , \tag{8b}$$

where the $f_{k,ab}$ are given by Eq. (5a). The F_{ab}^{type} are scaling factors. The β_{ab} are radiative branching ratios for line-to-line fluorescence transitions. These branching ratios are defined as the ratio of a specific radiative transition from the a emitting state to a specific b state divided by the sum of all the radiative transitions initiated from the a state of the kth Eu^{3+} configuration:

$$\beta_{k,ab}=\frac{A_{k,ab}^{\text{ems}}}{\sum_{a,b}A_{k,ab}^{\text{ems}}}\ , \tag{9}$$

where a represents a given emitting state and b represents lower energy states. The $A_{k,ab}^{\text{ems}}$ are the line-to-line radiative transition probabilities for the kth configuration as defined in Eq. (5b), and the sum is over all the possible lower states. The sum of all β_{ab} is necessarily equal to 1.

VIII. RESULTS AND DISCUSSION

A. Type of calculations and assumptions

Several choices had to be made before we calculated the optical spectra of Eu^{3+} ions doped in the simulated glass. These choices pertain to the type of calculation and to certain assumptions made in order to solve the crystal-field Hamiltonian of each Eu^{3+} configuration. Specifically, the following points had to be considered.

1. Point-charge crystal-field model

Several *ab initio* models for predicting the energy-level schemes of rare-earth ions doped in solid matrices have been successfully proposed: the electrostatic model,[34] the method of operator equivalents,[35] the superposition model,[36] the angular overlap model,[37] and molecular-orbitals calculations.[38] The choice of the point-charge crystal-field model based on the three-parameter theory developed by Leavitt, Morrison, and Wortman[15] is justified with regards to the type of molecular modeling we have performed. In effect, the MD technique, using a two-body potential, considered only electrostatic (ionic) interactions; no bond directionality is introduced with this type of potential to simulate covalent interactions or orbital overlap. Therefore, the use of ligand-field theory or molecular-orbital theory would not be justifiable in this context.

2. Point symmetry of the Eu^{3+} ion

As we have reported in a previous article,[12] none of the 150 glass configurations present a high degree of symmetry. This is normally expected due to the disordered nature of the glass matrix, which dictates that the lowest symmetry possible must prevail. As such, the point symmetry of the "sites" occupied by the rare-earth ions should be regarded as C_1. Brecher and Riseberg[1] used a

C_{2v} symmetry in their treatment of FLN spectra. The reasons they invoked were that (1) this was the highest symmetry in which the full splitting of the $^7F_1$ and $^7F_2$ levels is accounted for, (2) it is a subgroup of almost all the higher point symmetries and therefore allowed the application of the descending symmetries technique, and (3) it was, at that time, the lowest symmetry for which simple CF calculations could be performed. In the case at hand, the choice of a C_2 point symmetry for the rare-earth environment was dictated by similar considerations.

3. *Free-ion parameters*

When a rare-earth ion is placed into a solid-state lattice, the ion becomes influenced by the inhomogeneous electric fields arising from the presence of the atoms of the lattice (the so-called crystal-field). This causes the lifting of the degeneracy of the J levels of the free ion. The crystal-field Hamiltonian can actually be considered a perturbation of the free-ion Hamiltonian. Although the true energies of the free-ion are exceedingly difficult to obtain experimentally, the free-ion parameters in the Hamiltonian of the Eu^{3+} ion have been given based on an analysis of the spectrum of Eu^{3+} in aqueous solutions. Table III presents (1) values computed using the free-ion parameters found in Ref. 39 for the energy-level barycenters of Eu^{3+}, (2) the experimental barycenters of the J manifolds found for the absorption and emission spectra of the $Na_2O{\cdot}2SiO_2{:}Eu^{3+}$ laboratory glass, and the (3) barycenters of the J manifolds used, in the present simulation, adjusted in order to obtain a proper fit with experimental results.

4. *Lattice-summation technique*

In their original contribution on the simulation of rare-earth optical spectra, Brawer and Weber[7] only considered the ligands of the first coordination shell, i.e., F^- ligands that were found inside a sphere of 2.75 Å of radius with the Eu^{3+} lying at its center. They limited their calculations to the second-order parameters in the crystal-field expansion, which simplified the relationship between energy levels and glass structure. After verifying the behavior of the B_{2m} parameters with respect to distance from the rare-earth ion, we noticed that the crystal-field parameters converged to a given value only after a distance of ≈ 12 Å. This prompted us to take into account all the atoms in our simulated ensemble. This is closely related to the crystalline lattice-summation technique, where the electrostatic crystal field at an impurity site is determined by summing the contributions of all atoms in a given volume of crystallographic space. Such a calculation is feasible for a crystal because of the inherent translational symmetry of the unit cell. For an experimental glass this is impossible, since the unit cell is infinite. However, in the case of a computer-simulated glass, where atomic positions are known, such a calculation is possible.

TABLE III. Energy-level barycenters for various Eu^{3+} ions.

J manifold	E_{calc} (cm^{-1})[a]	E_{exp} (cm^{-1})[b]	E_{sim} (cm^{-1})[c]
$^7F_0$	0.0	0	0
$^7F_1$	381.0	380	350
$^7F_2$	1 049.5	961	925
$^7F_3$	1 911.9	1 980	1 939
$^7F_4$	2 897.9	3 055	3 000
$^7F_5$	3 958.7	3 842	3 886
$^7F_6$	5 060.2	4 922	4 882
$^5D_0$	17 316.6	17 275	17 228
$^5D_1$	19 057.3	19 008	19 000
$^5D_2$	21 529.8	21 523	21 500
$^5D_3$	24 420.7	24 440	24 390
$^5L_6$	25 406.3	25 450	25 375

[a]Fitted parameters for Eu^{3+} (aq) found in Ref. 39.
[b]Experimental barycenters of the $Na_2O{\cdot}2SiO_2{:}Eu^{3+}$ experimental glass.
[c]Best-fit parameters used for the $Na_2O{\cdot}2SiO_2{:}Eu^{3+}$ simulated glass.

5. *Stimulating the effects of covalency*

The last point of concern was the use of partial charges in the crystal-field calculation. While performing the calculations using Eq. (3) for rare-earth ions doped in several crystalline materials, Karayianis and Morrison[20] investigated the effects of varying the charges from their purely ionic values to partial charges. They found that the introduction of partial charges had a significant effect on the fitting of experimentally obtained energy levels. Effectively, the inclusion of partial charges used in a reanalysis of the optical spectra of a number of rare-earth ions in $CaWO_4$, resulting in a different interpretation of experimental data.[40] The inclusion of partial charges in the crystal-field calculation reduces the magnitude of the electrostatic interaction between atoms which leads to a simulation of the effects of covalency. This does not in any way constitute the introduction of a covalency term in the crystal-field calculation. In Fig. 1, we show the effect of the variation of the oxygen and silicon charges upon the simulated $^5D_0 \leftarrow {}^7F_0$ transition. We chose a value between -2.0 and -1.0 for the charge on the oxygen ions and kept the full charge value on the europium and sodium ions, so that the charges on the silicon were varied to maintain the electroneutrality of the whole ensemble of atoms. We observed the following trends with decreasing charge on the O^{2-} and the Si^{4+} ions: (1) a red shift of the maxima, (2) a narrowing of the peaks, (3) a decrease in the intensity of the peaks, and (4) the disappearance of the high-energy asymmetry. All of these observations are consistent with what one would observe from an increase in the covalency of the silicate framework. Thus the choice of ionic charges was dictated by how well we could reproduce the various spectral features. Firstly, we considered the position, width, and shape of the $^5D_0 \leftarrow {}^7F_0$ transition. The europium-doped sodium disilicate glass shows, for this transition (room-temperature absorption), the following features: (1) a maximum situated at 578.9 nm, (2) a pronounced asymmetry on the high-energy side of the band, and (3) an FWHM of 88 cm^{-1}, all of which are confirmed by the results of

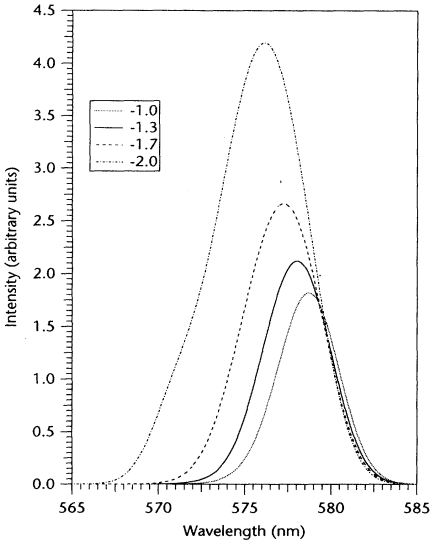

FIG. 1. Effect of variation of oxygen and silicon charges upon the simulated $^5D_0 \rightarrow {}^7F_0$ transition.

Kurkjian *et al.*[41] Secondly, we considered the width and shape of the $^5D_0 \rightarrow {}^7F_1$ transition with the specific intention of reproducing the noticeable splitting due to the triplet nature of the $^7F_1$ state. These considerations lead us to simulate the spectra with the following ionic charge values: (1) oxygen; -1.000, (2) silicon; $+1.485$, (3) sodium; $+1.000$, and (4) europium; $+3.000$. These values are in good agreement with the partial ionic charges for the SiO_4^{4-} tetrahedron reported by Pauling;[42] ($+1.06$ for the silicon atom and -1.27 for the oxygen atoms).

B. Simulated and experimental spectra

1. Absorption

Figure 2 shows a comparison between the absorption spectrum of the laboratory glass and that for the computer-generated $Na_2O{\cdot}2SiO_2{:}Eu^{3+}$ glass described in a previous article,[12] in the region between 350 and 600 nm. The simulated absorption spectrum shows only the $^5L_6$, $^5D_3$, $^5D_2$, $^5D_1$, $^5D_0 \leftarrow {}^7F_{0,1}$ transitions. These levels possess energies below 25 000 cm^{-1}, this being the limit where energy levels are still uncomplicated by extraneous mixing. The relative population of the $^7F_0$ and $^7F_1$ manifolds was taken into account in the simulated absorption spectrum by calculating the Boltzmann distribution at a temperature of 300 K. The simulated absorption line shape is seen to reproduce well the features of the experimental spectrum. Table IV presents a comparison between (1) the position of the barycenters, (2) widths, and (3) oscillator strengths of the simulated and experimental absorption spectra. One basis of comparison between the experimentally obtained absorption spectrum and the simulated spectrum is oscillator strengths. In order to compare the experimental values to simulated values calculated with Eq. (5a), we need to sum individual line-to-line simulated oscillator strengths (Eq. 5a) over all a and b components of J states A and B. The scaling factors of Eq. (8a) are also found in Table IV. These factors were chosen such that (1) the relative intensities of the simulated manifolds approximate those of the experimental manifolds and (2) the simulated oscillator strength of the $^5D_2 \leftarrow {}^7F_0$ transition is equal to that of the experimental transition. The $^5D_2 \leftarrow {}^7F_0$ transition was specifically chosen because of its relatively high optical density and because it is situated in a region free from interfering transitions. The scaling factors for transitions to the three lowest excited states are close to unity, whereas factors for the two highest excited states are approximately 4.5. The higher scaling factors in the latter case might be due to the presence of several transitions, in the 24 000–27 000 cm^{-1} region, which were not taken into account in the calculation. Because of broadening and overlap these unaccounted for transitions lend some intensity to the experimental transitions, forcing us to overcompensate the intensities of the calculated transitions for the sake of comparison.

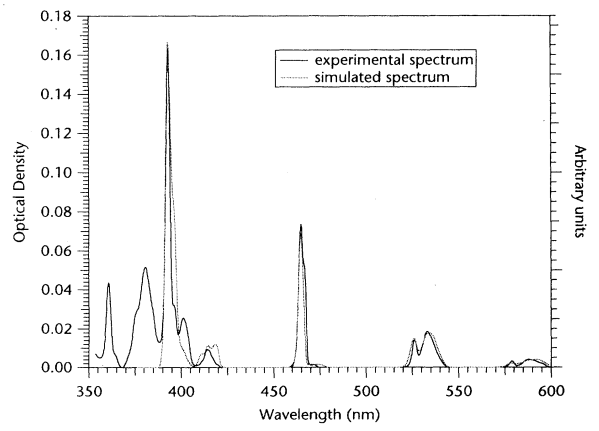

FIG. 2. Comparison between room-temperature absorption spectra of experimental and simulated Eu^{3+}-doped sodium disilicate glasses. The right-hand vertical axis represents the relative intensity (in arbitrary units) of the simulated absorption spectrum.

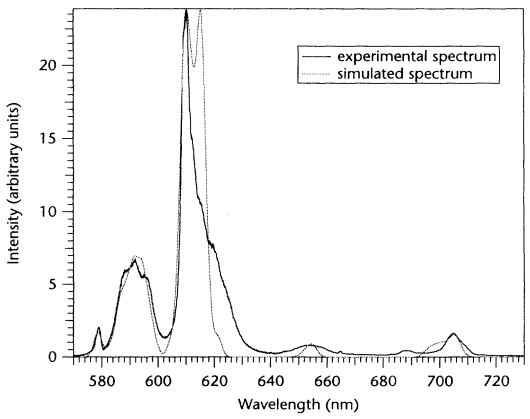

FIG. 3. Comparison between room-temperature emission spectra of experimental and simulated Eu^{3+}-doped sodium disilicate glasses.

TABLE IV. Absorption barycenters, linewidths, and oscillator strengths of the experimental and simulated $Na_2O{\cdot}2SiO_2{:}Eu^{3+}$ glasses. (Only the electronic transitions which have been simulated are reported.)

	$Na_2O{\cdot}2SiO_2{:}Eu^{3+}$ Experimental glass			$Na_2O{\cdot}2SiO_2{:}Eu^{3+}$ Simulated glass			
Assignment	Barycenter (cm^{-1})	FWHM (cm^{-1})	f ($\times 10^{-7}$)	Barycenter (cm^{-1})	FWHM (cm^{-1})	f ($\times 10^{-7}$)	Scaling factors[a]
$^5D_0 \leftarrow {}^7F_1$	16 978	321	0.105	16 901	328	0.064	1.32
$^5D_0 \leftarrow {}^7F_0$	17 275	88	0.030	17 282	102	0.028	1.32
$^5D_1 \leftarrow {}^7F_1$	18 758	260	0.459	18 704	236	0.253	1.32
$^5D_1 \leftarrow {}^7F_0$	19 008	94	0.148	19 008	150	0.209	1.32
$^5D_2 \leftarrow {}^7F_1$	21 189	b	0.030	21 144	b	0.029	1.32
$^5D_2 \leftarrow {}^7F_0$	21 523	230	1.207	21 528	120	1.212	1.32
$^5D_3 \leftarrow {}^7F_1$	24 143	280	0.285	24 128	372	0.227	4.42
$^5D_3 \leftarrow {}^7F_0$				24 436	b	0.067	4.42
$^5L_6 \leftarrow {}^7F_1$	c	c	c	25 076	b	0.233	4.62
$^5L_6 \leftarrow {}^7F_0$	25 450	191	3.494	25 444	212	5.624	4.62

[a]Factors defined in Eq. (8b).
[b]Indicates a shoulder.
[c]The presence of other transitions interferes with the identification of this band.

2. *Emission*

Figure 3 shows a comparison of the experimental and simulated emission spectrum of the $^5D_0 \rightarrow {}^7F_J$ ($J=0$ to 4) transitions for the same glasses. Although they have been calculated, the $^5D_0 \rightarrow {}^7F_{5,6}$ transitions are not shown in this figure for reasons of clarity.

We find in Table V a comparison of band positions, widths, and relative intensities for the simulated and experimental room-temperature emission spectra for the $Na_2O{\cdot}2SiO_2{:}Eu^{3+}$ glasses. The scaling factors of Eq. (8b) are also found in Table V.

Overall, a good qualitative agreement has been obtained for the positions and energy splittings of the simulated emission transitions. It is evident that discrepancies arise between the laboratory and simulated emission spectra. The most probable reason is due to the fact that we are simulating a "*static*" spectrum. We have considered the amorphous environment as merely supplying a static average electrostatic field. Any dynamic process which occurs in the laboratory sample, such as ion-lattice coupling (vibronic coupling) or ion-ion coupling (energy transfer), which affect specific aspects of the laboratory spectrum will necessarily be missing from the simulated spectrum. For example, Tables IV and V show the presence of a Stokes shift between the experimental $^5D_0 \leftarrow {}^7F_0$ absorption and $^5D_0 \rightarrow {}^7F_0$ emission transitions. Since we have not included a vibronic coupling term in the perturbation Hamiltonian, we are evidently not able to simulate such effects as Stokes shifts or vibronic sidebands.

Nevertheless, the model we present here fails in reproducing accurately the $^5D_0 \rightarrow {}^7F_2$ transition. As seen in Fig. 3, the overall intensity of the simulated $^5D_0 \rightarrow {}^7F_2$ transition is adequate, but we were not able to reproduce

TABLE V. Emission barycenters and linewidths of the experimental and simulated $Na_2O{\cdot}2SiO_2{:}Eu^{3+}$ glasses.

	$Na_2O{\cdot}2SiO_2{:}Eu^{3+}$ Experimental glass		$Na_2O{\cdot}2SiO_2{:}Eu^{3+}$ Simulated glass		
Assignment	Barycenter (cm^{-1})	FWHM (cm^{-1})	Barycenter (cm^{-1})	FWHM (cm^{-1})	Scaling factors[a]
$^5D_0 \rightarrow {}^7F_0$	17 288	75	17 282	102	5.5
$^5D_0 \rightarrow {}^7F_1$	16 901	375	16 901	328	2.0
$^5D_0 \rightarrow {}^7F_2$	16 314	355	16 328	272	1.0
$^5D_0 \rightarrow {}^7F_3$	15 306	285	15 289	114	1.1
$^5D_0 \rightarrow {}^7F_4$	14 215 14 524	155 100	14 233	254	1.0
$^5D_0 \rightarrow {}^7F_5$	(b)	(b)	13 352	224	5.0
$^5D_0 \rightarrow {}^7F_6$	12 344	215	12 349	148	0.07

[a]Factors defined in Eq. (8a).
[b]Barely observable transition.

the observed intensity distribution of the five Stark components of this transition. The five components of the experimental $^5D_0 \rightarrow {}^7F_2$ transition are situated at 15 982, 16 107, 16 255, 16 385, and 16 410 cm^{-1}. These have been determined by a least-squares minimization routine using Gaussian band shapes. It is clear that these five components have very different transition probabilities and thus contribute to the appreciable asymmetry of the $^5D_0 \rightarrow {}^7F_2$ transition. The simulated $^5D_0 \rightarrow {}^7F_2$ transition only shows three distinct components with unexpected relative intensities. The first, found at 16 088 cm^{-1}, corresponds to the 16 107 cm^{-1} component of the experimental transition. The second, found at 16 256 cm^{-1}, corresponds to the 16 255 cm^{-1} component of the experimental transition. The third component, found at 16 388 cm^{-1}, corresponds to the 16 385 and 16 410 cm^{-1} components of the experimental transition. One possible explanation for the apparent absence of certain energy components is the likelihood of other radiative transitions appearing in the same energy range of the experimental spectrum. The presence of $^5D_1 \rightarrow {}^7F_4$ transition components within the same energy range as the $^5D_0 \rightarrow {}^7F_2$ manifold has been observed in various solid-state hosts.[43] Nevertheless, it is very unlikely that radiative $^5D_1 \rightarrow {}^7F_4$ transitions appear in the experimental emission spectrum because of the presence of very efficient multiphonon processes in silicate glasses,[44] which induce nonradiative $^5D_1 \rightarrow {}^5D_0$ transitions. Disregarding this disparity in transition energies, the main problem still lies in the relative intensities of the various components of this simulated transition. In their theoretical treatment of the Eu^{3+} emission spectrum in $Na_3[Eu(oxydiacetate)_3]\cdot 2NaClO_4\cdot 6H_2O$, Morely, Saxe, and Richardson[45] observed that their calculations failed to account for the intensity distribution observed for the $^5D_0 \rightarrow {}^7F_2$ transition. They stated that the most likely explanation was found in an analysis of the dynamic coupling model reported by Kuroda, Mason, and Rossini.[46,47] This model was also previously shown to be identical to a mechanism based on an inhomogeneous dielectric medium surrounding the rare-earth ion.[48] Electrostatic interactions between the trivalent lanthanide ion and its surrounding environment can be divided into two categories. The first, static coupling, represents electrostatic interactions between the metal ion multipoles and the net charges of the ligand atoms. Only the ligand charges and atomic coordinates are used in this scheme. The second, dynamic coupling, represents electrostatic interactions between the metal ion multipoles and the multipoles of the ligand charge distribution. Isotropic ligand polarizabilities and atomic coordinates are normally used in this second scheme. Kuroda, Mason, and Rossini concluded that the presence of dynamic coupling and in particular the inclusion of ligand polarizability anisotropy was essential in the proper calculation of the electric dipole intensity distribution of transitions which exhibit quadrupole (Eu^{3+})-dipole (ligand) coupling mechanisms, such as the $^5D_0 \rightarrow {}^7F_2$ transition. In this study, only the static coupling scheme has been implemented in the calculation of the electric dipole strengths. It is evident that the inclusion of the dynamic coupling scheme, including ligand polarizability anisotropy, will resolve any discrepancies for transitions with an important electric quadrupole character.

C. Spectra-structure correlations

The ability to infer structural features from spectra has been, over the past few decades, one of the main goals of optical spectroscopy. Some success has been borne out of the study of doped crystals, nevertheless, any attempt to do so with glasses was seen to fail. Since we are not restricted by the direct study of an experimental spectrum, it is possible for us to establish an indirect link between a structural model of europium-doped sodium disilicate glass and the experimental spectra of the corresponding laboratory glass.

Using the simulated structural model of the Eu^{3+}-doped sodium disilicate glass, spectra-structure correlations will be investigated. Each will stem from the knowledge of the exact local atomic configurations surrounding each of the doped ions and by the possibility to identify and isolate individual structural contributions to the simulated spectra. This is exemplified in the following two figures. Figure 4 presents a graphic representation of a typical Eu^{3+} local environment. The ions displayed are those found in a sphere of 4.0 Å of radius centered at the position of the Eu^{3+} ion. The four atomic types of the simulated glass are represented in this figure, i.e., the central ion is the europium which is bonded to seven oxygens which are themselves attached to silicon atoms (the four smallest spheres), while the three sodium atoms are represented with no bonds. In this configuration, the average Eu-O bond length is 2.7 Å, calculated with a cutoff of 3.2 Å. Figure 5 shows the $^5D_0 \leftarrow {}^7F_{0,1}$ region of the simulated spectrum, with the exact energies of the Eu^{3+} configuration represented in Fig. 4 indicated by the four arrows.

In optical spectroscopy of glasses, it is common practice to examine the evolution of various spectroscopic features as a function of the excitation energy of an absorption band. As an example, features such as crystal-field parameters and their ratios, energy barycenters, radiative decay times of an emitting level, and Judd-Ofelt

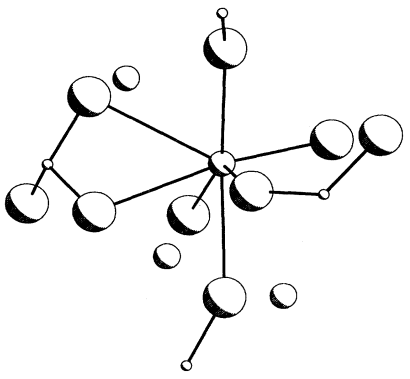

FIG. 4. Schematic representation of local environment of one of the 150 simulated Eu^{3+} ions.

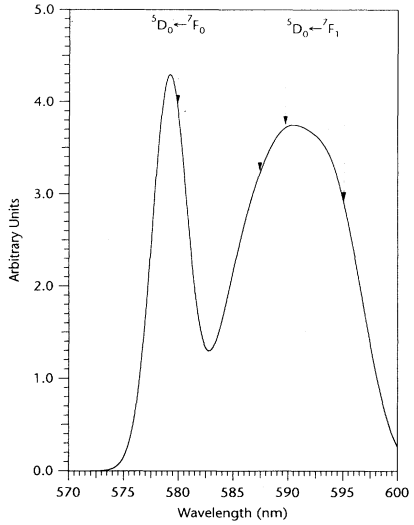

FIG. 5. $^5D_0 \leftarrow ^7F_{0,1}$ region of the absorption spectrum of the simulated Eu^{3+}-doped $Na_2O \cdot 2SiO_2$ glass. Arrows indicate location of transition energies for the Eu^{3+} configuration represented in Fig. 3.

parameters, have been examined through fluorescence line narrowing. This was interpreted as indirectly examining structural/spectral relationships in order to infer details of the local environment of the doped luminescent probe ions. We shall take the same approach and try to recreate some of these experimentally derived relationships.

1. *Influence of the crystal field*

The first relationship to be investigated is the possible influence of the crystal field on the barycenter energy of the Eu^{3+} J manifolds. To a first approximation (point-charge crystal-field model, no J mixing, no covalency terms or other correction terms to the perturbation Hamiltonian), the only effect the crystal field will have is to lift the degeneracy of the J manifold. Under this approximation, the barycenters of the J manifolds will be identical to the corresponding free-ion barycenters. Therefore, the only difference between two Eu^{3+} configurations will be in the amount of splitting of the respective J manifolds. The width observed, for transitions of rare-earth ions doped in a glass, could be interpreted as follows. Configurations having high-field strengths will show a large splitting and they will be sitting on either side of the inhomogeneously broadened band. Conversely, configurations having low-field strengths will have a small splitting and will be sitting in the middle of the inhomogeneously broadened band. Keeping with this approximation, a $J=0 \leftrightarrow J'=0$ transition, because the manifolds involved cannot be split, should show a width that corresponds to homogeneous broadening and should not show any inhomogeneous broadening. This is not the case for the $^5D_0 \leftrightarrow ^7F_0$ transitions of the trivalent europium ion doped in sodium disilicate (Figs. 2 and 3), nor is it true for any other Eu^{3+}-doped inorganic glass. This first approximation is thus inadequate to explain the width of such transitions and it is reasonable to assume that it is also inadequate for transitions where J and/or J' are different from 0. The question then remains. How does the crystal field affect the position of the individual manifold barycenters which make up the inhomogeneously broadened bands of doped glasses?

In order to investigate this point, the crystal-field strength S_{CF} [Eq. (7)] has been plotted versus the excitation wavelength (the position of the $^5D_0$ manifold representing the $^5D_0 \leftarrow ^7F_0$ transition) for each of the 150 Eu^{3+} configurations. This plot is shown in Fig. 6. In this figure, we observe a linear decrease, between 574.5 and 579 nm, of the crystal-field strength followed by a sharp fall. The general trend for this transition, could then be interpreted as a blue shift of the transitional energy with crystal-field strength. This blue shift could be construed as an indication of the overall covalency effect which was introduced in the crystal-field model by the inclusion of partial charges. This could be likened to the observation of a red shift of the transitional barycenter with a decrease in the oxygen partial charge, as observed in Fig. 1. Since the crystal-field strength is a representation of the electrostatic interaction between the rare-earth ion and its local environment, it could be expected that a decrease of the crystal-field strength is a representation of an increase in covalent interactions. However, since we have not formally introduced a covalent interaction term in the crystal-field Hamiltonian, it could be deemed improper to make such a statement.

In order to investigate further this indication of covalency, we have plotted the energy barycenters of the simulated $^5D_0 \rightarrow ^7F_J$ ($J=0-6$) transitions as a function of the crystal-field strength. These plots are shown in Figs. 7(a) and 7(b). Two horizontal lines are seen to cross each of the graphs. The dotted lines represent the energy of the free-ion barycenters (second column of Table III).

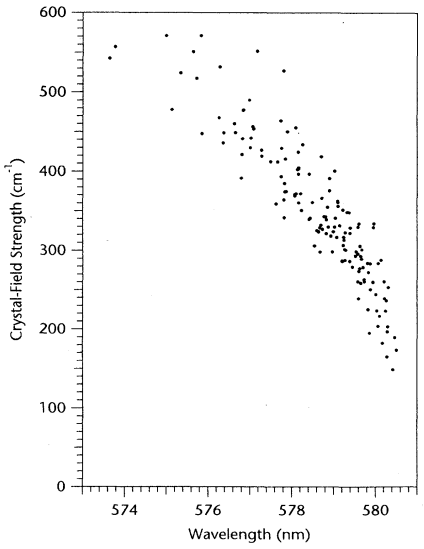

FIG. 6. Plot of crystal-field strength S_{CF} as a function of simulated $^5D_0 \leftarrow ^7F_0$ transition wavelength.

The full lines represent the energy of the simulated transitional barycenters (fourth column of Table V). Several general observations can be made of these figures. Firstly, the transitions do not present the same behavior towards crystal-field strength. The $^5D_0 \rightarrow {}^7F_{0,1,2,3,4}$ transitions present a blue shift of the barycenter energy with increasing crystal-field strength, whereas the $^5D_0 \rightarrow {}^7F_{5,6}$ transitions present a red shift of the barycenter energy with increasing crystal-field strength. Secondly, except for the $^5D_0 \rightarrow {}^7F_6$ transition, all the transitions present a decrease in the energy of the overall simulated barycenter when compared with the free-ion barycenter. This is likened to the experimental observation of the nephelauxetic effect seen in rare-earth doped crystals.[49] We must note that, since no covalency term has been included in the perturbation Hamiltonian, the nephelauxetic effect cannot be calculated by the present crystal-field model. However, this effect is observed because of the use of partial charges which red shift the position of the overall barycenters of each transition (Fig. 1). Thirdly, the magnitude of the energy shifts of the overall transitional barycenters are different from one level to another. The magnitude of the effect of the overall covalency should be different for each level.[50,51] Finally, it is observed that the magnitude and the shape of the crystal-field strength-dependent energy shift is different from one level to another.

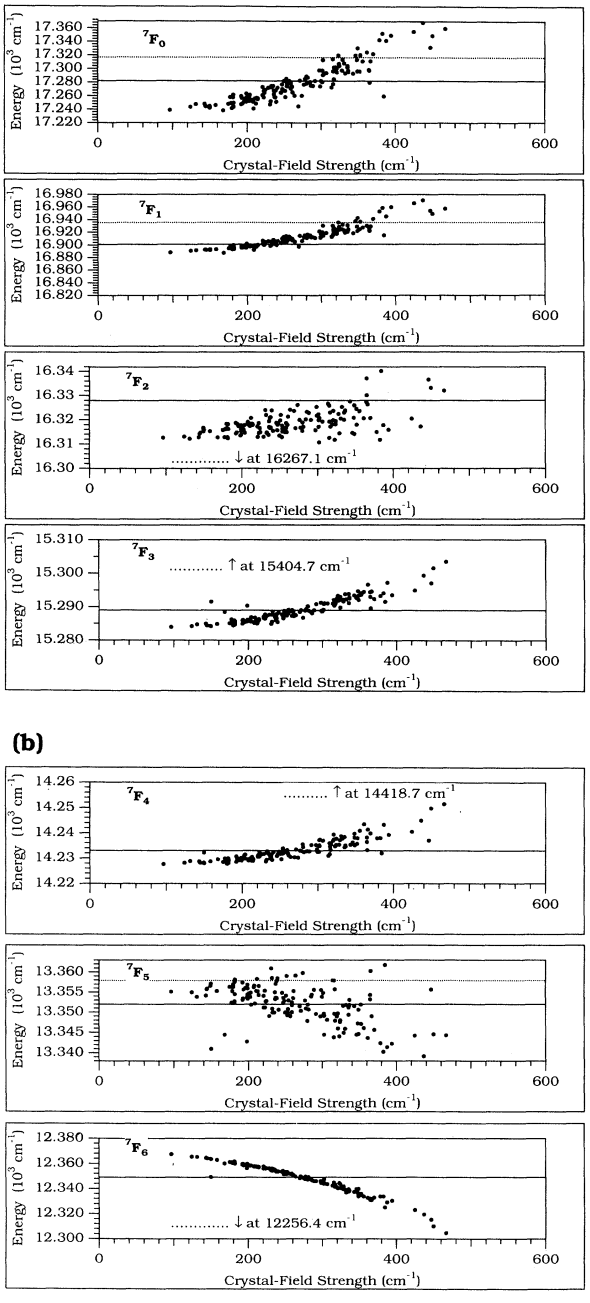

FIG. 7. (a) Energy barycenters for the $^5D_0 \rightarrow {}^7F_{0,1,2,3}$ transitions versus crystal-field strength. (b) Energy barycenters for the $^5D_0 \rightarrow {}^7F_{4,5,6}$ transitions versus crystal-field strength.

2. *J mixing*

The only factor included in the crystal-field model, which could explain all of the above-mentioned observations, is J mixing. J mixing is defined as the interaction (or mixing) of states belonging to different free-ion levels (which ordinarily have different J values). The influence of J mixing is usually considered small when the free-ion levels are relatively isolated as is the case for rare-earth doped crystals. Caro, Beaury, and Antic,[50] have shown that the effect of J mixing in Eu^{3+}-doped crystals is weak and is practically null for the $^5D_0$ level. In the present case, although the $^5D_0$ and ^7F_J states are well separated from one another, the individual J manifolds of the ^7F_J states are only separated by approximately 1000 cm^{-1}, from one to the next. As for the $^5D_0$ state, it is close to the $^5D_{1,2,3}$ and $^5L_6$ levels. All these manifolds show substantial overlap due to the disordered nature of the glass which also contributes significantly to the presence of J mixing. Since the crystal-field strength is directly responsible for any variation of the splitting of a J manifold, individual Stark levels will be at different energies from one Eu^{3+} configuration to another. Because of this, J mixing will also be different from one Eu^{3+} configuration to another, causing the observed shift in the energies of transitional barycenters. Also, since each J manifold presents a different amount of J mixing, each of the $^5D_0 \rightarrow {}^7F_J$ transitions will present a variation in the magnitude of the energy shift and a variation in overall behavior. In all probability, this is the reason for the observed blue shift of the $^5D_0 \rightarrow {}^7F_{0,1,2,3,4}$ transitions and the red shift of the $^5D_0 \rightarrow {}^7F_{5,6}$ transitions. Since the $^7F_{5,6}$ states are much closer to the $^5D_0$ state, this reversal could be explained by J mixing with the lower ^7F_J states and the higher $^5D_0$ state.

This is an observation of the influence of the crystal-field strength on J mixing. To verify this experimentally, one would need to separate the individual contributions of electrostatic interaction, covalency, J mixing, and a multitude of other effects.[52] This is complicated enough for rare-earth ions doped in crystals, it is deemed impossible for rare-earth ions doped in glasses. To investigate

the effect of J mixing theoretically, is also an insurmountable task. Specifically, to be able to predict the behavior of the energy of the barycenters of individual J states, due to a variation of J mixing with crystal-field strength, would require an enormous amount of computational time. When J mixing is taken into consideration in a crystal-field calculation, the matrix elements of all the possible $\alpha JM,\alpha' J' M'$ combinations must be calculated. In the present crystal-field calculation, where we have dealt *only* with the lowest 12 [SL] J states (which represent a total of 78 individual Stark levels) of the Eu^{3+} ion, the matrix of the perturbation Hamiltonian will have 78×78 elements, with 78 diagonal matrix elements and 6006 off-diagonal matrix elements. These off-diagonal matrix elements are responsible for the effect of J mixing.

Absorption and emission spectra of ions doped in glasses consist of bands which are broadened due to the superposition of contributions from individual ions distributed among the entire ensemble of local environments. This is the classical textbook definition of inhomogeneous broadening. Yet, very little is known about the microscopic origins of inhomogeneous broadening. To this definition, we might add that one of the main contributions to inhomogeneous broadening is due to the variation of J mixing amongst the entire ensemble of local environments.

D. Model for the rare-earth environment

As we can see in Figs. 8 and 9, there are no distinguishable correlations between the excitation energy and the numbers and average distances of the oxygen ligands surrounding the subsets of Eu^{3+} ions excited at a given energy. This leads us to believe that the presence of a limited number of distorted "sites" as discussed by various authors[41,53–60] is fallacious and that the rare-earth environments are rather composed of a continuous distribution of local-fields which satisfy energetic bonding requirements of the Eu^{3+} ions, while disregarding structural bonding requirements normally attributed to complexes or crystalline compounds. In this context, it is perfectly understandable that a Eu^{3+} ion surrounded by four oxygen ligands could experience the same crystal field as an eight-coordinated one; this has been previously referred to as "accidental degeneracies"[2] and must be more widespread than was thought of before. Another indication of the wide presence of these degeneracies is found in Fig. 6, where a vertical spread in CF strength values can be found for any given wavelength of excitation. That is to say that two or several Eu^{3+} configurations can have the same energy for the $^5D_0 \leftarrow {}^7F_0$ transition but still show drastic differences in their CF strength.

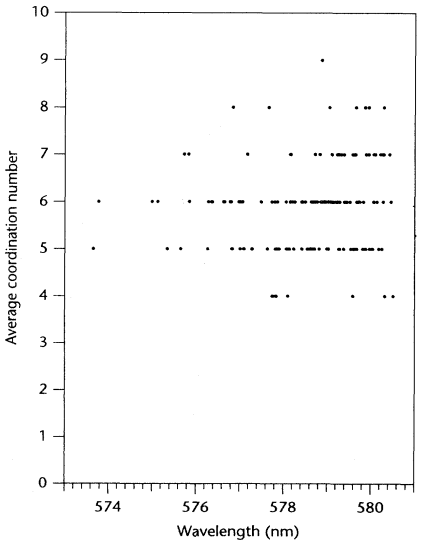

FIG. 8. Europium coordination number (oxygen ligands) as a function of the simulated $^5D_0 \leftarrow {}^7F_0$ transition wavelength.

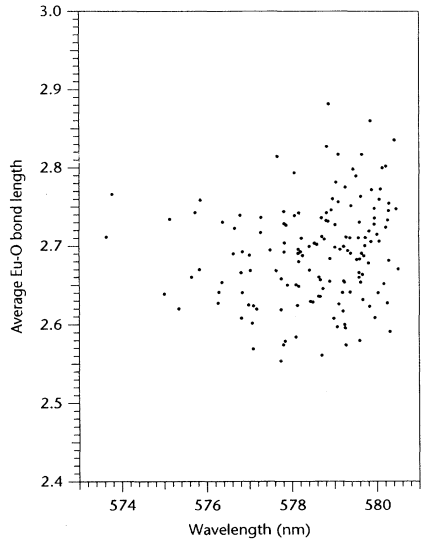

FIG. 9. Average ligand distance as a function of the simulated $^5D_0 \leftarrow {}^7F_0$ transition wavelength.

One possible exception to the previous discussion, is the likely presence of two limited distributions of "high-symmetry sites" found in Eu^{3+}-doped fluorozirconate glass.[61] Although the evidence presented is somewhat sketchy, the authors argue that they observe two major types of sites using site selection spectroscopy techniques. These sites, surprisingly, are thought to present high-symmetry elements, such as an inversion center. The explanation as to the difference in behavior of rare-earth ions doped in this type of glass, when compared to oxide glasses, was that the Eu^{3+} ions are acting as network formers rather than network modifiers. In the present context, we suggest that the two different distribution of sites present in this type of glass, arise from the Eu^{3+} ions present as two entirely different "species", i.e., network former and network modifier, and therefore found in two different types of local environments. This may lead to two different spectral responses which could be subsequently isolated.

In addition to coordination number and the spatial distribution of ligands, other factors will definitely influence the local field of a Eu^{3+} ion. Amongst them, we can cite

the following. Firstly, each oxygen ligand which is in the first coordination shell of the Eu^{3+} ion, will bring about various numbers of *"free"* negative charges. This is due to the fact that in an oxide glass, three possible types of oxygens can exist, namely, bridging, nonbridging or free. Secondly, the presence of network-modifying cations in close vicinity with the Eu^{3+} ion will affect the density of charge of the surrounding oxygens. Thirdly, the Eu^{3+} ion should be influenced by the magnitude of covalent interactions of the surrounding atoms (oxygen ligands, network modifiers, and the silicate framework). Figures 6 and 7 have shown that the crystal field varies with the excitation wavelength and we postulated that this was due to a variation of J mixing and indirectly to covalency. Individual structural factors such as local point-group symmetry, coordination number and average bond distances are known to have an important effect on the electronic spectra of rare-earth ions doped in crystals. As seen in Figs. 8 and 9, the Eu^{3+} coordination number and the Eu-O average bond distance have slight individual influences on the energy of the individual $^5D_0 \leftarrow {}^7F_0$ transitions. Since there is no symmetry involved in the make-up of the individual sites, this would tend to prove *a contrario* that no one individual structural factor greatly influences the electronic spectra of doped ions in inorganic glasses. Rather, we present evidence that it is the overall electrostatic and covalent energy of the individual sites together with the site-to-site variation of this energy which hold the greatest influence. To pursue this matter further, an extension of the structural and crystal-field models, i.e., the inclusion of a three-body potential in the MD simulation and the use of ligand-field theory or molecular-orbital calculations, would be dictated.

E. FLN vs dilution narrowed laser spectroscopy

FLN spectra of the $Na_2O{\cdot}2SiO_2{:}Eu^{3+}$ glass are essentially identical with those reported in various other oxide systems.[1–4] Qualitatively, the FLN spectra show resolvable Stark components for both the $^5D_0 \rightarrow {}^7F_1$ and $^5D_0 \rightarrow {}^7F_2$ transitions. The energies of the Stark components of the $^7F_1$ and $^7F_2$ multiplets are shown in Fig. 10 as a function of the $^5D_0$ excitation energy. An attempt to recreate the FLN spectra from the simulated glass structure was unsuccessful due to the extremely small number of Eu^{3+} configurations which we have examined in this simulation. In the laboratory glass, the 0.94 wt. % Eu_2O_3 concentration is equivalent to 8.79×10^{19} ions/cm^3. Since in the FLN experiment we are using a narrowband excitation of approximately 2 cm^{-1}, and the inhomogeneously broadened $^5D_0 \rightarrow {}^7F_0$ absorption band has a linewidth of $\approx$90 cm^{-1}, we are in effect averaging out the spectral contributions of $\approx 1.5\times10^{18}$ emitters at the maximum of the band and of roughly 5×10^{16} emitters at its tail (positioned at 10% of the maximal intensity of the Gaussian). For the simulated glass, the sample size which corresponds to the 2-cm^{-1} bandwidth of the exciting laser, is typically 1 or 2 Eu^{3+} configurations. Although there is a definite selectivity in FLN spectra of experimental glasses, the experiment still corresponds to the investigation of a "macroscopic" behavior of a doped glass. The use of extremely narrow excitation sources, such as the FLN experiments performed by Selzer *et al.*,[62] with a spectral resolution of 20 MHz, confirms these points. In this experiment, no discontinuities were found in the FLN spectra, confirming the presence of a continuous distribution of local fields which could not be resolved into the contributions of individual "sites." Due to this, any attempts to infer structural information from these experiments is bound to be complicated by the fact that one is looking at an overwhelming amount of accidental degeneracies. Seeking "uniqueness" in a structural model for doped inorganic glasses might well be futile.

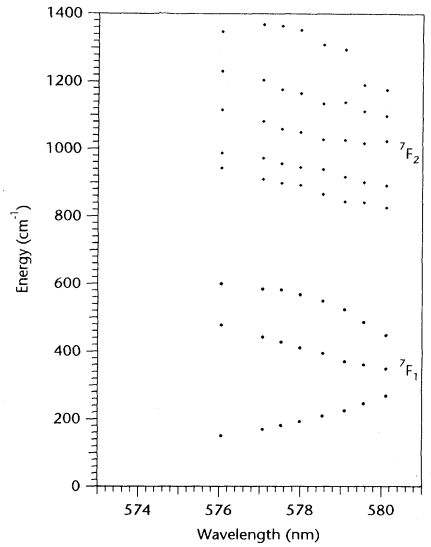

FIG. 10. Energy of Stark components of $^7F_{1,2}$ emissions as a function of excitation wavelength as determined by fluorescence line narrowing on the laboratory Eu^{3+}-doped $Na_2O{\cdot}2SiO_2$ glass.

Although we have not been able to simulate FLN spectra for the $Na_2O{\cdot}2SiO_2{:}Eu^{3+}$ glass, we are still able to derive various features normally associated with FLN spectroscopy. Shown in Fig. 11(a) are the positions of the three $^7F_1$ and five $^7F_2$ Stark levels for each of the 150 Eu^{3+} configurations as a function of the excitation energy. In Fig. 11(b), we show the same plot with data points which were averaged out from Stark levels of configurations having approximately the same excitation energy. These results present Stark splittings for the $^7F_1$ and $^7F_2$ manifolds which are equivalent in magnitude and position to those presented in Fig. 10.

The "macroscopic" behavior discussed above for FLN spectroscopy is to be distinguished from the "microscopic" behavior resulting from the extremely small sample size which is found for doped simulated glass. The latter behavior results in spectra very much akin to those obtained from the dilution narrowed laser spectroscopy (DNLS) technique developed by Yen and co-workers.[63] With the present technique of spectral simulation, it is possible to generate DNLS spectra by reducing considerably the associated linewidths [the w factor of Eq. (7)] of the simulated transitions. Investigations into the simula-

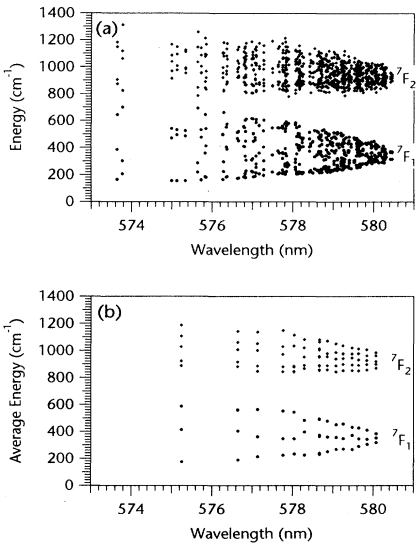

FIG. 11. Energy of Stark components of $^7F_{1,2}$ emissions as a function of the simulated excitation wavelength. (a) Representation of 150 Eu^{3+} configurations, (b) averaged energies of Eu^{3+} configurations.

tion of DNLS results will be the subject of a future article.

IX. CONCLUSIONS

The molecular-dynamics technique has allowed us to simulate a model of Eu^{3+} ions doped in a sodium disilicate glass. Using crystal-field theory, we have calculated the electronic energy levels and transition probabilities of the simulated Eu^{3+} ions, resulting in the simulation of absorption and emission spectra. By comparing the simulated spectra with experimental spectra, we were able to validate the proposed simulated structural model, allowing us in turn to investigate spectra-structure correlations of doped inorganic glasses.

We have found no distinguishable correlations between the excitation energy and the numbers and average distances of the oxygen ligands surrounding the simulated Eu^{3+} ions. This leads us to conclude that the presence of a limited number of distorted sites for rare-earth ions doped in oxide glasses is now thought to be fallacious. The rare-earth environments are rather composed of a continuous distribution of local-fields which satisfy energetic bonding requirements of the Eu^{3+} ions, while disregarding structural bonding requirements normally attributed to complexes or crystalline compounds.

ACKNOWLEDGMENTS

We wish to thank Dr. Marco Bettinelli and Dr. Peter Taylor for the glass samples and their absorption spectrum. We are grateful to Dr. Richard P. Leavitt and to Gregory Turner for the original version of the crystal-field calculation programs. The authors wish to thank Dr. M. J. Weber for very helpful discussions. We also gratefully acknowledge the Natural Science and Engineering Research Council of Canada for financial support. One of the authors (G.C.) is grateful for support from the Natural Science and Engineering Research Council of Canada and the Fonds pour la Formation de Chercheurs et l'Aide à la Recherche (Québec). Also, one of us (A.M.) thanks the Centre Jacques-Cartier for a grant.

*Author to whom correspondence should be addressed.

[1]C. Brecher and L. A. Riseberg, Phys. Rev. B **13**, 81 (1976).
[2]M. J. Weber, in *Laser Spectroscopy of Solids,* 2nd ed., edited by W. M. Yen and P. M. Selzer (Springer-Verlag, Berlin, 1986), p. 189.
[3]J. A. Capobianco, P. P. Proulx, and N. Raspa, Chem. Phys. Lett. **160**, 591 (1989).
[4]J. A. Capobianco, P. P. Proulx, M. Bettinelli, and F. Negrisolo, Phys. Rev. B **42**, 5936 (1990).
[5]C. Brecher and L. A. Riseberg, Phys. Rev. B **21**, 2607 (1980).
[6]S. A. Brawer and M. J. Weber, Phys. Rev. Lett. **45**, 460 (1980).
[7]S. A. Brawer and M. J. Weber, J. Non-Cryst. Solids **38&39**, 9 (1980).
[8]S. A. Brawer and M. J. Weber, J. Lumin. **24/25**, 115 (1981).
[9]M. J. Weber and S. A. Brawer, J. Non-Cryst. Solids **52**, 321 (1982).
[10]M. J. Weber and S. A. Brawer, J. Phys. (Paris) Colloq. **43**, C9-291 (1982).
[11]M. J. Weber, J. Non-Cryst. Solids **73**, 351 (1985).
[12]G. Cormier, J. A. Capobianco, and A. Monteil, J. Non-Cryst. Solids **142**, 225 (1993).
[13]L. V. Woodcock and K. Singer, Trans. Faraday Soc. **67**, 12 (1971).
[14]C. Nelson, T. Furukawa, and W. B. Nelson, Mater. Res. Bull. **18**, 959 (1983).
[15]R. P. Leavitt, C. A. Morrison, and D. E. Wortman, *Rare Earth Ion-Host Crystal Interactions 3. Three Parameter Theory of Crystal-Fields,* Harry Diamond Laboratories Report TR-1673 (June 1975); U.S. National Technical Information Service, Springfield, VA, Report No. A017849.
[16]C. A. Morrison and R. P. Leavitt, J. Chem. Phys. **71**, 2366 (1979).
[17]C. A. Morrison, D. E. Wortman, and R. P. Leavitt, J. Chem. Phys. **73**, 749 (1980).
[18]C. A. Morrison, D. E. Wortman, and R. P. Leavitt, J. Chem. Phys. **73**, 2580 (1980).
[19]N. Karayianis and C. A. Morrison, *Rare Earth Ion-Host Crystal Interactions 1. Point charge lattice sum in Scheelites,* Harry Diamond Laboratories Report TR-1648 (October 1973); U.S. National Technical Information Service, Springfield, VA, Report No. AD-776330/3.
[20]N. Karayianis and C. A. Morrison, *Rare Earth Ion-Host Crystal Interactions 2. Local distortion and other effects in reconciling lattice sums and phenomenological B_{km},* Harry Diamond Laboratories Report TR-1682 (January 1975); U.S. National Technical Information Service, Springfield, VA, Report No. A011252.
[21]S. K. Mitra, Philos. Mag. B **45**, 529 (1982).
[22]S. K. Mitra and R. W. Hockney, Philos. Mag. B **48**, 151 (1983).

[23]R. L. Mozzi and B. E. Warren, J. Appl. Cryst. **2**, 164 (1969).
[24]G. N. Greaves, A. Fontaine, P. Lagarde, D. Raoux, and S. J. Gurman, Nature (London) **293**, 611 (1981).
[25]C. A. Morrison and R. P. Leavitt, in *Handbook on the Physics and Chemistry of Rare-Earths,* edited by K. A. Gschneider and L. Eyring (North-Holland, Amsterdam, 1982), Chap. 46.
[26]C. A. Morrison, *Crystal-Fields for Transition-Metal Ions in Laser Host Materials* (Springer-Verlag, Berlin, 1992).
[27]R. P. Leavitt, J. Chem. Phys. **77**, 1661 (1982).
[28]E. U. Condon and G. H. Shortley, *The Theory of Atomic Spectra* (Cambridge University Press, Cambridge, England, 1957).
[29]B. R. Judd, Phys. Rev. **127**, 750 (1962).
[30]G. S. Ofelt, J. Chem. Phys. **37**, 511 (1962).
[31]C. A. Morrison, R. P. Leavitt, J. B. Gruber, and N. C. Chang, J. Chem. Phys. **79**, 4758 (1983).
[32]W. F. Krupke, Phys. Rev. **145**, 325 (1966).
[33]See, for example, R. E. Christoffersen, *Basic Principles and Techniques of Molecular Quantum Mechanics* (Springer-Verlag, Berlin, 1989), Chap. 3.
[34]M. T. Hutchings and D. K. Ray, Proc. Phys. Soc., London **81**, 663 (1963).
[35]K. W. H. Stevens, Proc. R. Soc. London, Ser. A **65**, 209 (1952).
[36]M. M. Curtis, D. J. Newman, and G. E. Stedman, J. Chem. Phys. **50**, 1077 (1969).
[37]C. K. Jörgensen, J. Phys. **26**, 825 (1965).
[38]M. M. Curtis and D. J. Newman, J. Chem. Phys. **52**, 1340 (1969).
[39]W. T. Carnall, P. R. Fields, and K. Rajnak, J. Chem. Phys. **49**, 4412 (1968).
[40]R. P. Leavitt, C. A. Morrison, and D. E. Wortman, J. Chem. Phys. **61**, 1251 (1974).
[41]C. R. Kurkjian, P. K. Gallagher, W. R. Sinclair, and E. A. Sigety, Phys. Chem. Glasses **4**, 239 (1963).
[42]L. Pauling, *The Nature of the Chemical Bond,* 3rd ed. (Cornell University, Ithaca, 1960), p. 321.
[43]See, for example, C. Brecher, H. Samelson, R. Riley, and A. Lempicki, J. Chem. Phys. **49**, 3303 (1968); J. P. Morley, J. D. Saxe, and F. S. Richardson, Molec. Phys. **47**, 379 (1982).
[44]C. B. Layne, W. H. Lowdermilk, and M. J. Weber, Phys. Rev. B **16**, 10 (1977).
[45]J. P. Morley, J. D. Saxe, and F. S. Richardson, Molec. Phys. **47**, 379 (1982).
[46]R. Kuroda, S. F. Mason, and C. Rosini, Chem. Phys. Lett. **70**, 11 (1980).
[47]R. Kuroda, S. F. Mason, and C. Rosini, J. Chem. Soc. Faraday Trans. 2, **77**, 2125 (1981).
[48]B. R. Judd, J. Chem. Phys. **70**, 4830 (1979).
[49]C. K. Jögensen, *Modern Aspects of Ligand Field Theory* (North-Holland, Amsterdam, 1971).
[50]P. Caro, O. Beaury, and E. Antic, J. Phys. (Paris) **37**, 671 (1976).
[51]C. K. Jörgensen, Struct. Bonding (Berlin) **25**, 2 (1976).
[52]C. A. Morrison, *Angular Momentum Theory Applied to Interactions in Solids,* Lecture Notes in Chemistry Vol. 47 (Springer-Verlag, New York, 1988).
[53]S. Mockovciak, J. Pantoflicek, and K. Patek, Phys. Status Solidi **11**, 401 (1965).
[54]S. K. Barber, in *Interaction of Radiation with Solids,* edited by A. Bishay (Plenum, New York, 1967), p. 593.
[55]D. K. Rice and L. G. DeShazer, Phys. Rev. **186**, 387 (1969).
[56]M. M. Mann and L. G. DeShazer, J. Appl. Phys. **41**, 2951 (1970).
[57]J. T. Fournier and R. H. Bartram, J. Phys. Chem. Solids **31**, 2615 (1970).
[58]C. C. Robinson, J. Non-Cryst. Solids **15**, 1 (1974); **15**, 11 (1974).
[59]R. Reisfeld and Y. Eckstein, J. Solid State Chem. **5**, 174 (1972).
[60]R. Reisfeld and N. Lieblich, J. Phys. Chem. Solids **34**, 1467 (1973).
[61]J. L. Adam, V. Ponçon, J. Lucas, and G. Boulon, J. Non-Cryst. Solids **91**, 191 (1987).
[62]P. M. Selzer, D. L. Huber, D. S. Hamilton, W. M. Yen, and M. J. Weber, in *Structure and Excitations in Amorphous Solids,* edited by G. Lukovsky and F. L. Galeener, AIP Conf. Proc. No. 31 (AIP, New York, 1976), p. 328.
[63]W. M. Yen, Third International Conference on Trends in Quantum Electronics, edited by A. M. A. Prokhorov and I. Ursu [SPIE J. **1033**, 183 (1988)].